JACS
JOURNAL OF THE AMERICAN CHEMICAL SOCIETY
pubs.acs.org/JACS
Article

Fast Photoswitchable Molecular Prosthetics Control Neuronal Activity in the Cochlea

Aida Garrido-Charles,△ Antoine Huet,△ Carlo Matera,△ Anupriya Thirumalai, Jordi Hernando, Amadeu Llebaria, Tobias Moser,* and Pau Gorostiza*

Cite This: J. Am. Chem. Soc. 2022, 144, 9229–9239
Read Online
ACCESS | Metrics & More | Article Recommendations | Supporting Information

ABSTRACT: Artificial control of neuronal activity enables the study of neural circuits and restoration of neural functions. Direct, rapid, and sustained photocontrol of intact neurons could overcome the limitations of established electrical stimulation such as poor selectivity. We have developed fast photoswitchable ligands of glutamate receptors (GluRs) to enable neuronal control in the auditory system. The new photoswitchable ligands induced photocurrents in untransfected neurons upon covalently tethering to endogenous GluRs and activating them reversibly with visible light pulses of a few milliseconds. As a proof of concept of these molecular prostheses, we applied them to the ultrafast synapses of auditory neurons of the cochlea that encode sound and provide auditory input to the brain. This drug-based method afforded the optical stimulation of auditory neurons of adult gerbils at hundreds of hertz without genetic manipulation that would be required for their optogenetic control. This indicates that the new photoswitchable ligands are also applicable to the spatiotemporal control of fast spiking interneurons in the brain.

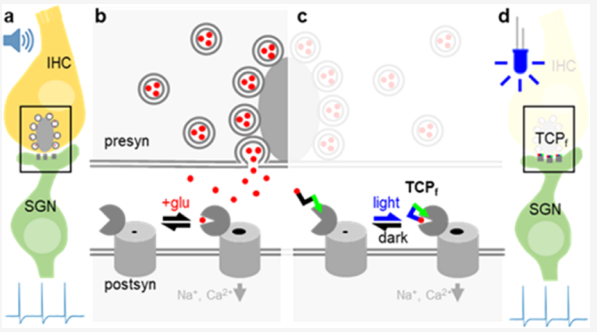

INTRODUCTION

Ultrafast signaling is a feature of several important neural circuits such as those in the auditory pathway, the brainstem, the cerebellum, and the cerebrum.[1−3] Such signaling builds on specialized synapses for synchronous neurotransmission as well as on suitable neural membrane properties for speedy action potential generation and propagation. The resulting neural firing features high rates and submillisecond precision. For an example, synaptic sound encoding builds on ultrafast glutamatergic transmission at specialized ribbon synapses formed by inner hair cells (IHCs) achieving firing at rates of several hundreds of hertz with submillisecond precision in spiral ganglion neurons (SGNs).[4,5] Utmost precision of the neural time code of the incoming sound forms the basis of sound localization in dedicated neural circuits of the brainstem that feature powerful calyceal synapses and neurons with extremely short membrane time constants owing to their specialized set of ion channels.[1,2]

Dissecting the function of such time-critical neural circuitries requires ultrafast control of neuronal activity. Likewise, functional restoration, for example, following degeneration of the sensory receptor cells, needs bionic approaches that reinstate the physiological information processing as closely as possible. Restoration of hearing to the deaf currently employs electrical stimulation of SGNs by cochlear implants (CIs).[6−8] Due to wide spread of current from each electrode contact, encoding of sound frequency information is heavily limited in CIs. Moreover, electrical SGN stimulation results in supernatural synchronization of neural activity and hence CIs employ high rates to generate pseudostochasticity of SGN firing. Recently, optogenetics has been proposed for improved bionic SGN stimulation, as light can be better confined in space. Rapidly gating channelrhodopsins enable optogenetically evoked firing with near-physiological temporal fidelity. Yet, genetic manipulation for expression of channelrhodopsins presents a risk to consider. Avoiding the need for gene therapy, photopharmacology could help reduce the complexity of optical SGN stimulation. Reversibility of chemical photoswitches[9] makes them interesting candidates for controlling neural excitation via endogenous neuronal receptors, such as ionotropic glutamate receptors (GluRs) of the postsynaptic SGN boutons in the cochlea.

Photoswitchable tethered ligands (PTLs) are covalently attached to their receptor and seem particularly attractive for this purpose. If conjugated precisely, they can provide finer photocontrol than freely diffusible photochromic ligands. PTLs produce higher local concentrations[10] and cannot diffuse away,

Received: November 22, 2021
Published: May 18, 2022

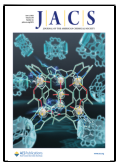

https://doi.org/10.1021/jacs.1c12314
J. Am. Chem. Soc. 2022, 144, 9229−9239

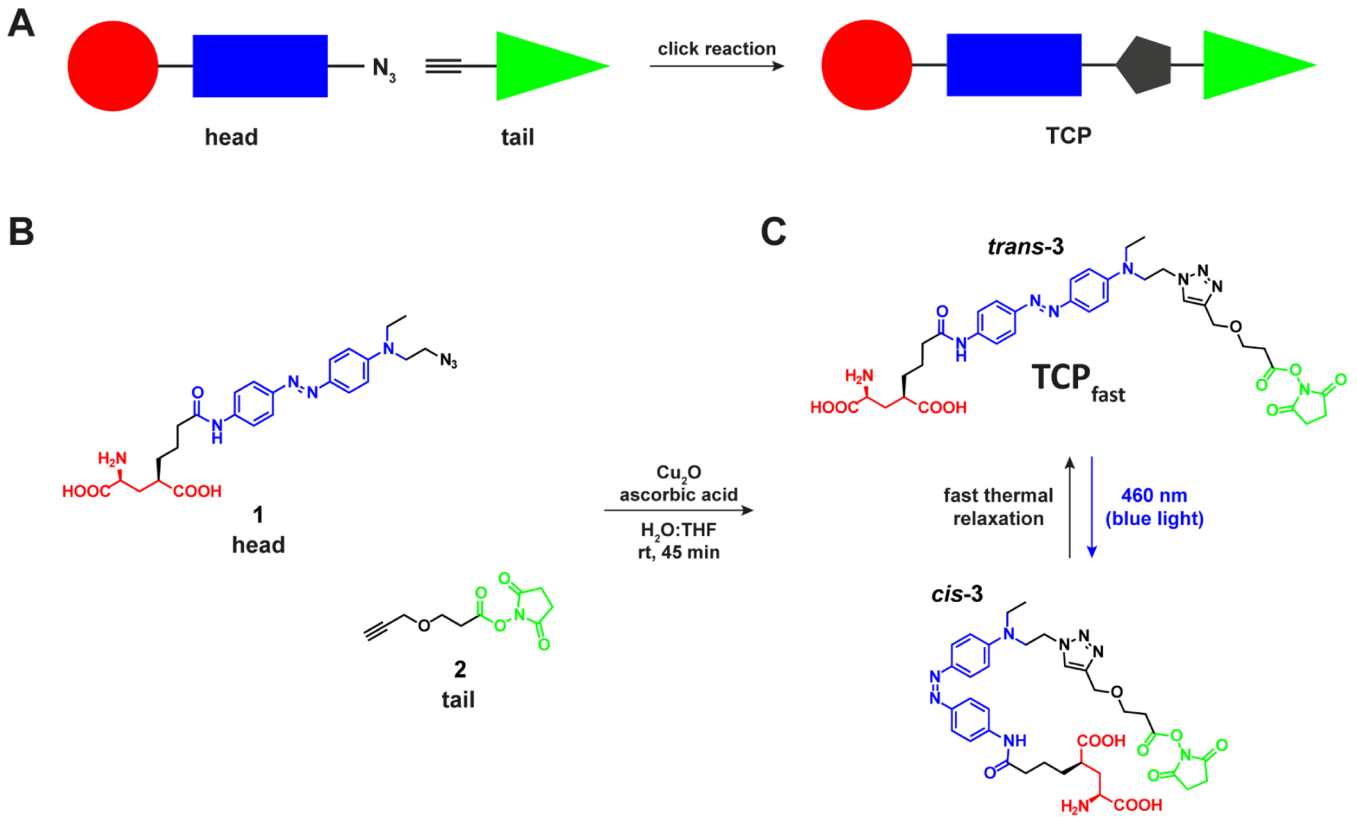

Figure 1. Fast-relaxing targeted covalent photoswitch of endogenous GluRs. (A) Schematic representation of the click chemistry strategy adopted for the preparation of TCP ligands. Modular parts are the ligand (red), the photoswitch (blue), and the reactive anchoring group (green). (B) Molecular design showing "head" (**1**) and "tail" (**2**) precursors of TCP_{fast} (**3**) that are freshly coupled via a copper(I)-catalyzed azide−alkyne cycloaddition prior to incubation in neuronal tissue. (C) Chemical structure and photoisomerization of TCP_{fast} between the cis (blue light, λ = 460 nm) and trans (dark, fast relaxation) conformations.

which yields a sharper separation in biological activity between the two isomeric states.[11,12] Genetic manipulation can be avoided with affinity-labeling conjugation of PTLs to target nucleophilic residues in the native protein (e.g., lysine,[13] histidine[14]). These targeted covalent photoswitches (TCPs) can be applied to intact neurons and readily provide photocontrol for hours.[13] However, they display some limitations. The standard bistable photoswitches can be isomerized in milliseconds using dual-color light flashes (UV−visible), but these wavelengths penetrate poorly in tissue and are problematic in vivo. In addition, their slow-relaxing photochromism (lifetime ∼80 min for TCPs) limits to ∼80% the fraction of trans isomer that can be achieved with light[15−19] and thus the reversibility of effects. To address these shortcomings, photoswitches have been modified to isomerize with longer wavelengths and rapidly relax in the dark to 100% trans,[22,26] but these compounds were designed to target genetically modified receptors instead of the native proteins,[13] which has so far hindered their use in one-wavelength applications to ultrafast synapses and in vivo preparations. Thus, methods for direct, rapid, and sustained photocontrol of activity in intact neurons constitute an unmet need, both to study neuronal circuits for basic research purposes and to explore new phototherapies. Interestingly, when sensory cells or neurons are damaged or absent, fast and sustained neurotransmitter release is impaired, but the postsynaptic neurons and receptors can retain their full capacities (activation kinetics, localization, and complex formation with regulatory proteins) for extended periods of time, offering untapped potential for functional restoration.[6]

Here, we developed a fast-relaxing glutamate TCP (TCP_{fast}, Figure 1) that fulfills the abovementioned requirements. We show the ability of TCP_{fast} to produce photocurrents in naive hippocampal neurons likely via tethering to endogenous GluRs and reversibly modulating their activity with visible light pulses as short as a few milliseconds. As an original proof of concept, we demonstrate the application of this molecular tool to the ultrafast first synapses of the auditory system that mediate cochlear sound encoding. This drug-based method affords ultrafast rate stimulation of SGNs in naive adult gerbils, matching the performance of optogenetic photostimulation that requires gene therapy. In general, these photoswitches provide a fundamental resource of broad interest to spatiotemporally control endogenous receptors in intact neuronal circuits with ultrafast signaling.

RESULTS AND DISCUSSION

Design and Synthesis of a Fast-Switching TCP of Ionotropic GluRs. The molecular design of TCP_{fast} was based on the recently reported TCPs[13] and is shown in Figure 1A. TCPs have a modular structure obtained by combining an affinity "head" (**1**), which bears both the bioactive ligand (glutamate moiety) and the modified photoisomerizable unit (azobenzene), and a reactive "tail" (**2**) bearing the protein anchoring group (NHS ester). NHS ester-activated linkers are short-lived groups that promptly react with primary amines (e.g., lysine residues) under neutral or slightly alkaline

https://doi.org/10.1021/jacs.1c12314
J. Am. Chem. Soc. 2022, 144, 9229−9239

Scheme 1. Chemical Synthesis of the "Head" Module (1) Bearing the Glutamate Moiety, the Photoswitchable Unit, and the Terminal Azide

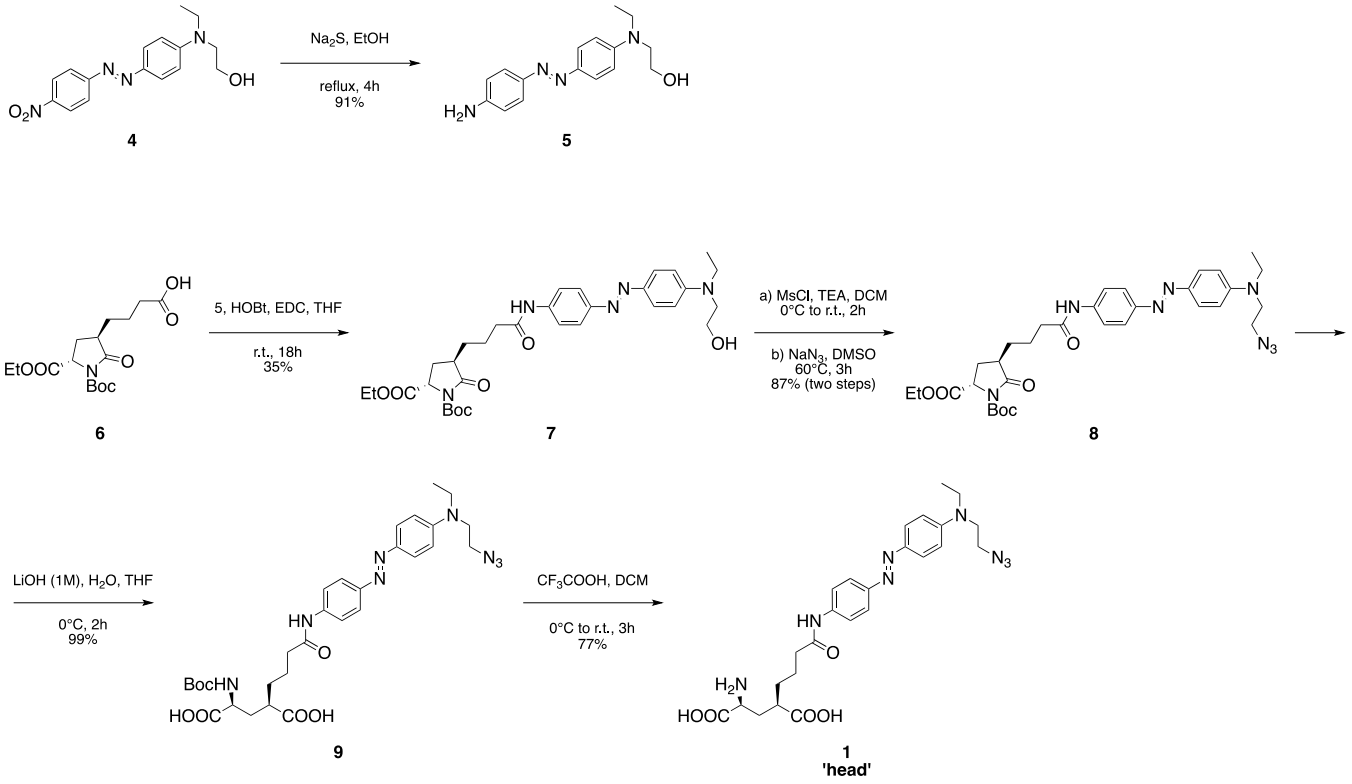

conditions (pH 7.2−9). To avert self-reactivity, TCPs are readily generated prior to attachment to the target protein via a copper(I)-catalyzed azide−alkyne cycloaddition reaction (CuAAC, also known as "click chemistry") (Figure 1B).

Previous TCPs featured azobenzene moieties that were photoisomerized using two different illumination wavelengths (380 and 500 nm) and characterized by slow thermal cis-to-trans relaxation.[13] Azobenzenes displaying faster relaxation kinetics and single, longer wavelength switching can be obtained with minimal variation of their chemical structure by generating an electron "push−pull" system. It consists of including connected electron donating groups on one aromatic ring of the azo unit and electron withdrawing groups on the other, which lower the energy barrier of the thermal cis-to-trans isomerization,[20,21] increasing the photoisomerization rate. This also results in a red-shifting of the azobenzene absorption spectrum, which is useful to reduce light scattering in tissue and phototoxicity, which is lower for longer wavelengths in applications in vivo. Thus, we designed a TCP_{fast} head in which one of the two amide groups at the para positions of the azobenzene was replaced by a tertiary amine as the electron-donating group.[22] To avoid perturbing the ligand region, we chose to introduce this modification on the opposite side of the azobenzene core (head compound **1**). Compound **1** was prepared via a five-step synthesis starting from commercially available materials (Scheme 1). Azobenzene **5** was obtained by reduction of its nitro precursor **4** with sodium sulfide nonahydrate. Pyroglutamate derivative **6**, prepared as previously described,[15] was coupled to compound **5** using HOBt/EDC activation to give the intermediate **7** and then converted via mesylation into the corresponding azide derivative **8**. Hydrolysis of the pyroglutamate moiety with concomitant saponification of the ethyl ester provided the advanced intermediate **9**, which was finally converted into the desired compound **1** via removal of the *tert*-butoxycarbonyl protecting group under acidic conditions (see also the Supporting Information for further details). This photoswitch showed an absorption maximum at about 460 nm (blue light) in aqueous solution at neutral pH (Figure S8), as previously reported.[22] Moreover, no variation of the absorption spectrum could be detected by steady-state UV−vis spectroscopy, suggesting that the cis isomer rapidly (<1 s) relaxes back to trans when the light is turned off. We used transient absorption spectroscopy to confirm photoswitching in aqueous phosphate buffer saline (PBS) solution, to measure the absorption spectrum and optimal wavelength of isomerization (450−460 nm), the relaxation lifetime in the dark (∼8 ms), and to demonstrate the high fatigue resistance of the compound (Figures S9−S11). The head (**1**) was coupled via CuAAC with a commercial tail (compound **2**) providing a fast-relaxing and red-shifted ligand (**3**) with a similar length to the successful TCP9 ligand previously described[13] (Figure 1C). To reach a satisfactory head-tail click coupling rate in minutes at room temperature, we replaced the conventional sodium ascorbate by ascorbic acid (see the Supporting Information for details). We hypothesized that the buffering effect of the ascorbic acid (to the tertiary amine in compound **1**) could create more proper pH conditions to promote the catalytic cycle of the reaction[23] as well as favor the formation of active copper(I) species from the copper(I) oxide catalyst.[24] Because NHS-based ligands are constitutively short-lived, we confirmed the formation of the desired TCP_{fast} by liquid chromatography−mass spectrometry (LC−MS) of the click reaction crudes and verified their ability to conjugate primary amine-containing biomolecules by reacting them with pure lysine as a mock protein residue (see the Supporting Information for details).

https://doi.org/10.1021/jacs.1c12314
J. Am. Chem. Soc. 2022, 144, 9229−9239

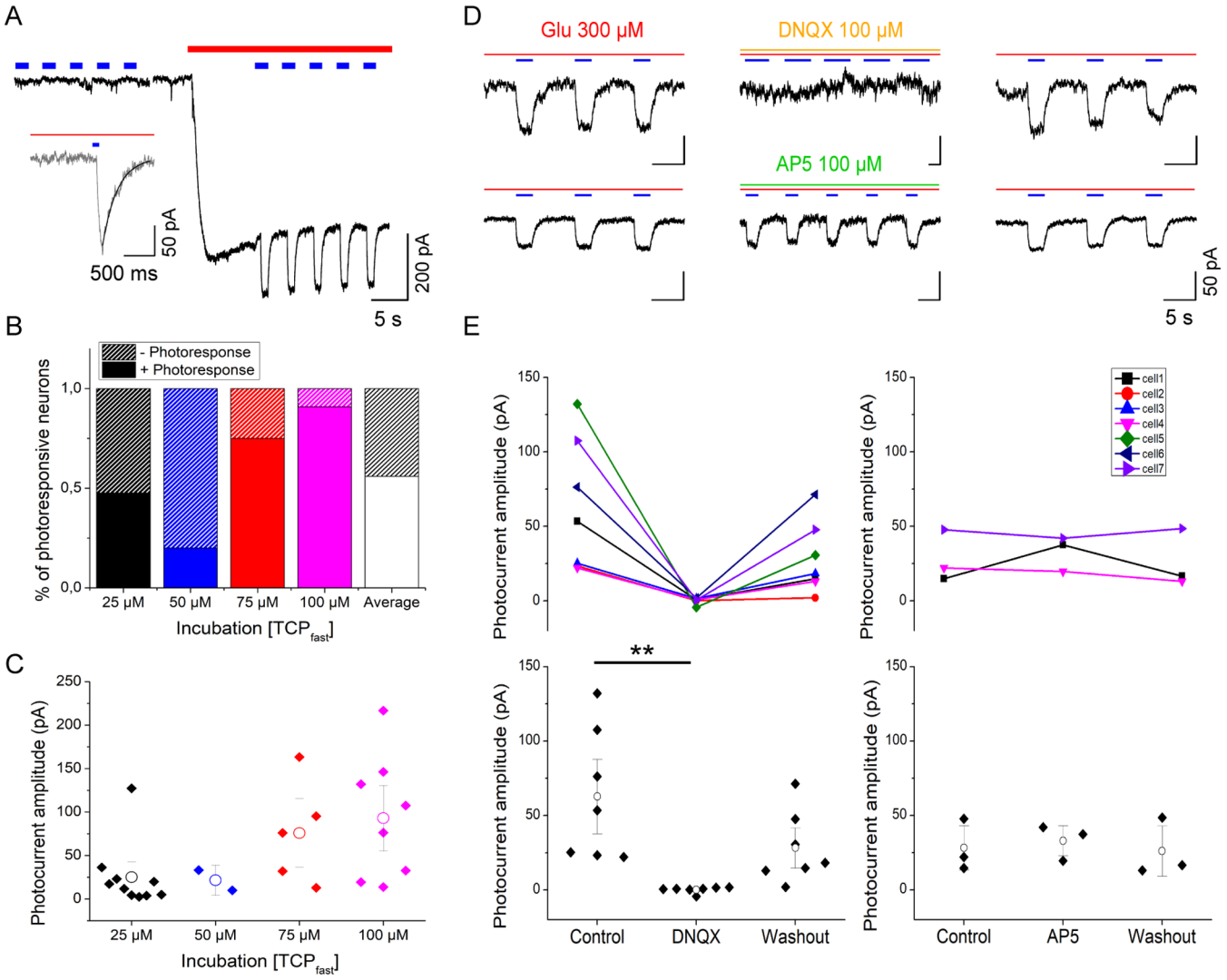

Figure 2. TCP_{fast} conjugation produces photocurrents in untransfected hippocampal neurons in the presence of glutamate via endogenous non-NMDA GluRs. (A) Current recording in whole cell voltage clamp mode in dissociated hippocampal neurons after incubation in TCP_{fast} (100 μM for 2 min at pH9). Inward current induced by bath perfusion of 300 μM glutamate (red bar) and 473 nm light (blue bars, 1 s). Time gap between traces corresponds to immediate subsequent recordings (<2s). Inset: photocurrent elicited by 100 ms light pulse. Exponential fit indicated in black correspond to Toff. (B) Increasing TCP_{fast} concentration during incubation (2 min, pH9, 25−100 μM) leads to a higher fraction of cells displaying photoresponses. (C) Photocurrent amplitude increases relative to concentration of TCP_{fast} incubated. Note: from the total number of cells responding to perfusion of 300 μM glutamate, 56% had light response. Per concentration, 47, 62% of cells incubated at 25 μM had light response (n = 21); 20% of cells incubated at 50 μM had a light response (n = 10); 75% of cells incubated at 75 μM had a light response (n = 8); 90% of cells incubated at 100 μM had a light response (n = 11). Means comparison by the Bonferroni test: 25 μM vs 50 μM (ns. p-value = 0.149); 25 μM vs 75 μM (ns; p-value = 0.198); 25 μM vs 100 μM (*, p-value = 0.0154); 50 μM vs 75 μM (*, p-value = 0.018); 50 μM vs 100 μM (**p-value = 2.6×10^{-4}); and 75 μM vs 100 μM (ns, p-value = 0.3758). (D) Current recordings in whole cell voltage clamp mode in rat hippocampal neurons maintained 15 days in culture and incubated with TCP_{fast} (100 μM for 2 min at pH 9). Example traces of photocurrents elicited by irradiation at λ_{ex} = 473 nm (1 s, blue bars) in the presence of 300 μM glutamate (red bar). Photocurrents are reversibly blocked by perfusion of 100 μM DNQX (orange bar) and not affected by 100 μM AP5 (green bar). After washout and reperfusion of 300 μM glutamate photocurrents are recovered, indicating covalent conjugation. Note that the absence of sharp responses may be indicative of GluR desensitization as a result of the high glutamate concentration. (E) Quantification of the effect of DNQX (100 μM, n = 7, p-value = 0.008) and AP5 (100 μM, n = 3, p-value = 0.56) on the photocurrent amplitude obtained from hippocampal neurons incubated with TCP_{fast} (25-75-100 μM for 2 min at pH9). Control and wash-out measurements were obtained after bath solution and glutamate perfusion. White dots indicate mean ± SE. Note: p-values obtained after performing Friedman test: non-parametric, data from any distribution; small samples; and related samples.

Characterization of TCP_{fast} in Cultured Neurons. We made use of the several GluRs subunits expressed by hippocampal neurons[25] to evaluate, on dissociated neuron cultures, the ability of TCP_{fast} to photocontrol GluR activity. TCP_{fast} was conjugated to GluRs by using the same incubation conditions (i.e., 2 min at 25−100 μM, pH 9 to favor deprotonation and reactivity of nucleophilic residues in the receptors, followed by wash-out of physiological solution, pH 7.4) previously shown to be favorable for TCP conjugation.[13] 473 nm illumination did not elicit photocurrent measured by whole-cell patch-clamp recordings directly after incubation with TCP_{fast}. However, in the additional presence of glutamate (300 μM), 473 nm illumination elicited 2.5−220 pA photocurrents (Figure 2A). As intended by the chemical

https://doi.org/10.1021/jacs.1c12314
J. Am. Chem. Soc. 2022, 144, 9229−9239

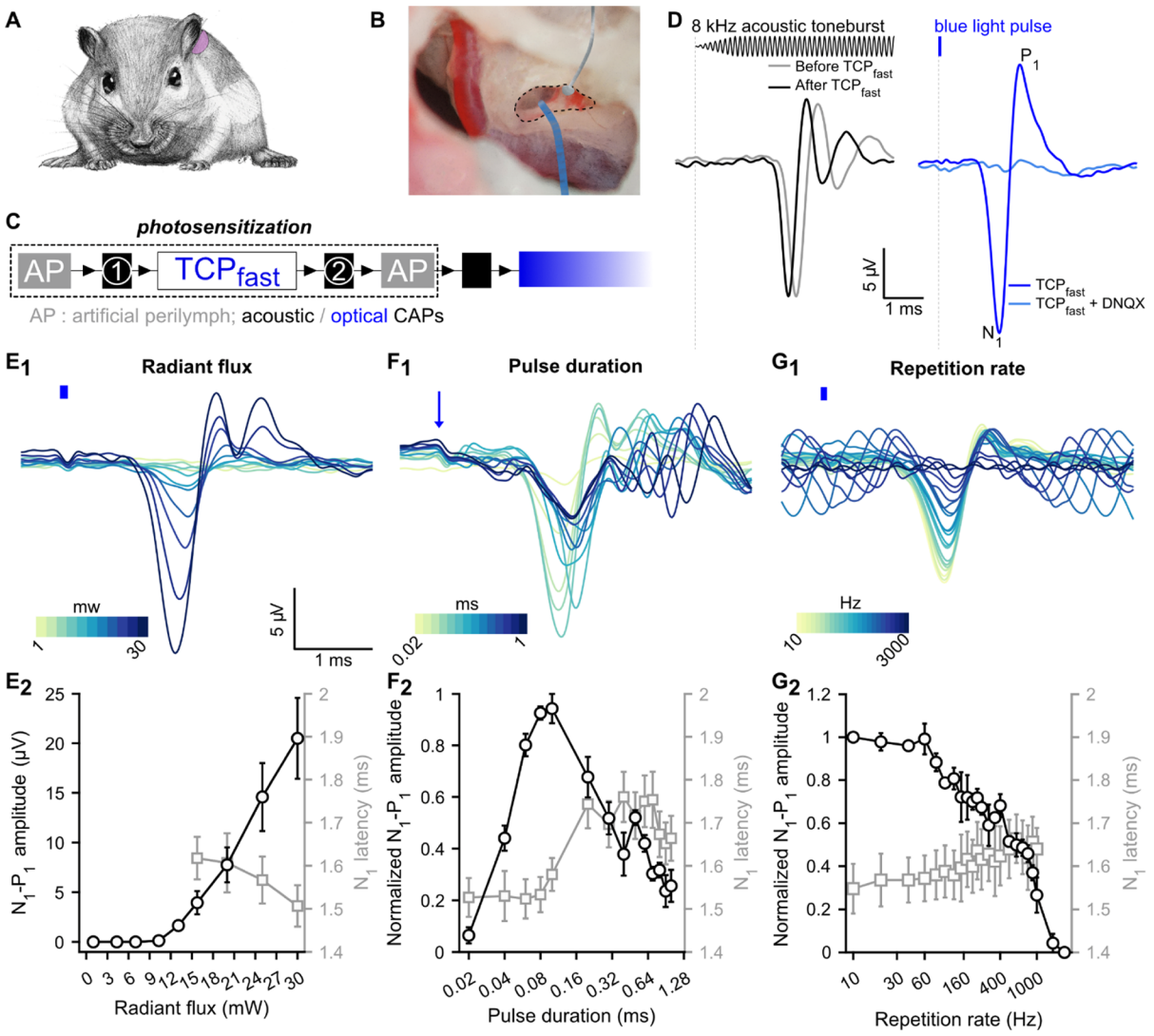

Figure 3. Fast photoswitchable control of SGN activity mediated by TCP_{fast}. (A) Mongolian gerbil cochlea was exposed, through the middle ear, by performing a retro-auricular approach. (B) Silver ball electrode was placed in the RW niche (dashed line) to record CAP in response to sound or to light stimulation. The light stimulation was delivered to the cochlea via an optical fiber coupled to a 470 nm-laser. (C) Experiment time course description: TCP_{fast} application (2.5−12.5 μM, 10 min) is preceded and followed by artificial perilymph application (AP) and acoustically CAP measurements. After the second AP application, the optical fiber is inserted in the RW and the optically evoked potentials (E−J) are recorded. (D) Representative acoustically (black, left, aCAP) and optically evoked CAP (blue, right, oCAP) following 2.5 μM application of TCP_{fast}. aCAPs (black, 200 averages, 8 kHz toneburst, 30 dB SPL, repetition rate = 20 Hz) are similar before and after TCP_{fast} application. oCAP (blue, 80 μs, 30 mW, repetition rate = 10 Hz) is abolished following application of competitive antagonist DNQX (1 mM). Stimuli are represented at the top. (E_1,G_1) Representative oCAP in response to various radiant fluxes (80 μs at 10 Hz, E_1), pulse durations (27 mW at 10 Hz, F_1), and repetition rates (80 μs at 27 mW, G_1). In (E_1,G_1), the blue line indicates the light stimuli and in F_1 the blue arrow indicates the beginning of the light pulse. A color scale is used to represent the variable. (E_2,G_2). Quantification (n = 6 cochleae) of the oCAP amplitude (N_1−P_1, black axis) and oCAP latency (N_1, gray axis) as a function of the radiant flux (E_2), the pulse duration (F_2), and the repetition rate (G_2). In F_2 and G_2, oCAP amplitudes were expressed as relative to the highest amplitude recorded for the given measure.

design, the cis isomer of TCP_{fast}, induced by blue light illumination, evoked inward photocurrents. thus supporting the notion that TCP_{fast} enabled fast-one-wavelength photomodulation of GluRs (Figure 2A inset). Next, we tested the effect of light in absence of TCP_{fast} incubation (Figure S16). The currents measured at the onset of 300 μM glutamate perfusion were of similar amplitude in both cases (793 ± 131 pA with TCP_{fast} and 1161 ± 445 pA without TCP_{fast}), discarding any non-specific effect of light stimulation. Direct perfusion of TCP_{fast} in the dark indicates that trans-TCP_{fast} can activate GluRs as a free ligand, an effect that is enhanced by light stimulation (Figure S17).

Next, we showed that the number of photosensitized hippocampal neurons (Figure 2B) and the amplitude of the photocurrent evoked by blue light (Figure 2C) increased with TCP_{fast} concentration during the incubation (25, 50, 75, and 100 μM). At 25 μM of TCP_{fast}, 47.62% of neurons (n = 21) had a measurable photocurrent (on average: 25 ± 12 pA), while 100 μM raised this to 90% of the neurons (n = 11) with a photocurrent of 93 ± 25 pA. In contrast, the relaxation lifetime in the dark of TCP_{fast}-conjugated neurons was independent of TCP_{fast} concentration and amounted to 220 ± 48 ms (Figures 2A inset and S18). As intended by our chemical design, the achieved relaxation lifetime was faster

https://doi.org/10.1021/jacs.1c12314
J. Am. Chem. Soc. 2022, 144, 9229−9239

than shown for TCPs (~80 min)[13] and comparable to one-wavelength PTLs (MAG_{460}: 710 ms,[22] MAG_{2P}: 150 ms and $MAGA_{2P}$: 265 ms[26]). For a subset of neurons, we also found that the photocurrent increased in amplitude with the radiant flux (Figure S19) and could be evoked by light pulse as short as 3 ms (Figure S20).

Finally, we showed that the photoresponses can be reversibly blocked by the AMPA receptor antagonist DNQX (100 μM) but not by the NMDA receptor antagonist AP5 (100 μM) (Figure 2D,E). This demonstrates that TCP_{fast} photocurrents are receptor-specific and that the photoswitchable ligands are indeed covalently tethered to GluRs (as the TCP_{fast}-mediated photoresponses persist even after washout and competition with an antagonist).

In Vivo Photocontrol of Neural Activity in Gerbil's Cochlea. The potential of TCP_{fast} to photosensitize SGNs in vivo was tested in the Mongolian gerbil cochlea using the same TCP_{fast} batch produced under the same click reaction conditions as for the in vitro characterization demonstrated above. The goal was to administer TCP_{fast} to SGNs, where it could covalently tether to the AMPA receptors in the postsynaptic density.

To do so, we surgically exposed the cochlea by performing a middle ear surgery (posterior tympanotomy) and applied TCP_{fast} to the niche of the round window (RW, a membrane-covered bony window of the cochlea, Figure 3A,B) for passive diffusion into the cochlea. In order to evaluate the potential toxicity induced by TCP_{fast}, we recorded cochlear mass potentials evoked by sound, before, during, and after TCP_{fast} diffusion. These mass potentials reflect the status of three cochlear cell types: outer hair cells, inner hair cells, and SGNs (for details, see Supporting Information, Figure 3C, Figure $S21A_{1-4}$). In this experiment, the acoustically evoked potentials reflecting the outer hair cells (i.e., the cochlear microphonic, Figure S21A3,B), IHCs (i.e., the summating potential, Figure S21A4,C), and SGNs (i.e., the compound action potential, CAP, Figure S21A4,D) remained largely unchanged following a 10 min application of 12.5 μM TCP_{fast} (0.25% of organic solvent) and wash-out (n = 4, Friedman's test). This indicates that TCP_{fast} incubation did not interfere with cochlear physiology.

We then tested for a TCP_{fast}-mediated photopharmacological SGN stimulation by inserting an optical fiber coupled to a blue laser (λ = 473 nm) into the RW. Transient optically evoked CAPs (oCAPs) were recorded from 12 out of 12 cochleae treated with TCP_{fast}. oCAPs were similar in shape to acoustically evoked CAP and had a maximal amplitude of 40.88 ± 12.58 μV (at maximum radiant flux: 30 mW), which is equivalent to the amplitude of a 50 dB SPL tone burst (Figure S21E). oCAPs vanished within minutes of optical stimulation, which was accompanied by a disappearance of the acoustic potentials reflecting the IHC and SGNs activation. The number of synapses per IHC (i.e., the juxtaposition of pre- [CtBP2] and postsynaptic [Homer 1] markers) was similar between treated and non-treated cochleae, at all frequencies, arguing against glutamate excitotoxicity induced by TCP_{fast}—mediated optical stimulation (Figure S21F-G and Supporting Method S2 for details). We can only speculate about a putative functional impairment of IHCs, SGNs, and their synapses, which might involve mechanisms such as phototoxic damage, for example, via generation of free radicals and desensitization and/or endocytosis of AMPA receptors. Future studies will be needed to elucidate such mechanisms. Interestingly, when we employed a lower TCP_{fast} dose (2.5 μM, <0.05% of organic solvent), we observed stable acoustically and optically evoked cochlear potentials in 60% of the incubated cochleae (Figures 3D−G, S22A−C). The other 40% of the cochleae were similar to previously reported using the highest concentration with a loss of mass potentially (Figure S22D−F), which indicates a narrow therapeutic window.

For the positive cochleae, oCAPs were similar in shape and amplitude to aCAP evoked by a 40 dB SPL toneburst but consistently showed a shorter latency (~1.5 ms, Figure 3D) indicating a direct optical SGN excitation bypassing the outer and middle ear transmission and inner ear mechanotransduction of sound in acoustic hearing. oCAPs could be abolished by DNQX (1 mM) application at the RW, supporting a response mediated by AMPA receptors (Figure 3D, light blue trace).

We further characterized the TCP_{fast}-mediated optical response by measuring oCAP amplitude and latency as a function of radiant flux (n = 6) using 80 μs light pulses at a repetition rate of 10 Hz (Figure 3E1,2). oCAP threshold amounted to 12.5 ± 0.62 mW (1 ± 0.05 μJ). From there, oCAP amplitude increased linearly with radiant flux up to 20.5 ± 4.09 μV at 30 mW and latency decreased from 1.62 ± 0.05 to 1.51 ± 0.05 ms. Next, we measured the effect of the pulse duration on the oCAP (Figure 3F1,2, 30 mW, repetition rate = 10 Hz): the biggest oCAPs were recorded in response to 80 and 100 μs light pulses. From there, oCAPs decreased in amplitude for shorter and longer durations. In 50% of the cases, sizable oCAPs (i.e., > 1 μV) were measured in light pulses as short as 20 μs, corresponding to 0.6 μJ. In response to light pulses shorter than 100 μs, oCAPs were characterized by a single negative wave occurring at ~1.54 ms. In contrast, oCAPs evoked by a longer pulse had multiple negative peaks, which might reflect the firing of multiple synchronous action potential across SGNs in response to the longer stimuli. Finally, we measured the effect of the repetition rate on oCAPs using 80 μs light pulses (Figure 3G1,2, 30 mW). The oCAPs were stable in amplitude up to 60 Hz and decreased exponentially at a higher repetition rate until not being observable for rates exceeding 1 kHz (the best performer cochlea is illustrated in Figure S23). The reported in vivo data support the concept of fast control of the AMPA receptor with TCP_{fast} in the SGNs.

CONCLUSIONS

In this work, we developed a chemical-biological method, called TCP_{fast}, which allows fast photoswitching of neuronal activity in native neurons. TCP_{fast} is a photoswitchable ligand that is chemically attached to endogenous receptors at the postsynaptic side.[13] The molecular design of TCP_{fast} optimized the properties of the bistable photoisomerizable group of former TCPs,[13] that is, thermal relaxation lifetime and absorption wavelength, without altering the ligand and the reactive group. TCP_{fast} functions as a molecular prosthesis that bypasses the neurotransmitter-encoded signal by a photonic signal. Photosensitization of cochlear SGNs by locally administered TCP_{fast} enabled temporally precise light-evoked SGN firing up to a rate of approximately 1 kHz, thus matching the fastest optogenetic SGN stimulation (≤1 kHz[27]). Hence, TCP_{fast}-mediated photopharmacology might serve as an interesting alternative to the optogenetic approach[6,28] for the development of an optical CI.

TCP_{fast} elicited depolarizing photocurrents that are activated by the cis isomer ("cis-on"), which is generally preferred to

https://doi.org/10.1021/jacs.1c12314
J. Am. Chem. Soc. 2022, 144, 9229−9239

avoid activation in the dark. Such behavior has been reported for similar photoswitchable ligands[10,13] and has been attributed to compound lengths and conjugation sites in the protein that allow ligand binding to the active site only in a "bent" (cis) conformation.[29] Molecular docking studies (Figures S25 and S26) and the cis-on agonist behavior of the freely diffusible compound in neurons (Figure S17) agree with this view. TCP_{fast} photoresponses are reversed in the absence of illumination with a thermal relaxation lifetime ranging between 8 ms for the TCP_{fast} head in the cuvette (Figure S9) and 220 ms in hippocampal neurons in culture (Figure S18). While slower lifetimes have been observed upon photoswitch conjugation and interaction with the target protein,[26] we can currently only speculate on how such a thermal relaxation rate measured in vitro yields the ultrafast photostimulation of SGNs in vivo eliciting SGN CAPs with interstimulus intervals ranging from a few milliseconds to submillisecond. Of note, postsynaptic boutons of SGNs likely contain hundreds of AMPARs such that each light stimulus might hit a sufficient number of AMPARs with the TCP_{fast} being in the trans state. Moreover, CAPs represent population responses and so light pulses might be recruiting variable subsets of SGNs. Finally, AMPA receptor desensitization might contribute to the transient response properties. Future work could consider to further speedup thermal relaxation potentially by replacing the current azobenzene unit in TCP_{fast} with faster photoswitches such as (hydroxy-substituted) phenylazopyrimidine (millisecond to nanosecond range[30−32]). However, such accelerated back-switching might in turn result in a lower cis conversion percentage in the photostationary state and, therefore, would require higher light intensity. In addition, further increasing the wavelength for photoswitching[33] might improve the overall utility of the method due to better tissue penetration and lower phototoxicity risk.

We demonstrated, in dissociated hippocampal neurons, specific photomodulation of AMPA/kainate receptors by TCP_{fast}. Such specificity is due to the affinity-labeling mechanism of PTLs.[10,13,29] In this experimental setting, TCP_{fast} photomodulation required the presence of glutamate in the bath solution for all the tested concentrations (Figure 2C), but in the range of 0.03−3 mM free glutamate, a weak correlation with the photocurrent amplitude was observed. One explanation could be that conjugated TCP_{fast} acts as a trans-on antagonist. However, because tethered glutamate has never been reported to act as an antagonist in GluRs and freely diffusible TCP_{fast} acts as an agonist, we argue that the requirement of glutamate is due to incomplete conjugation of TCP_{fast} to a heterogeneous population of endogenous GluRs. This concept may be translated into a distinctive subunit occupancy resulting in differential agonist affinity and efficacy, thus reducing the channel open probability (gating).[12,34,35] Enhancing the reactivity of the electrophilic group could improve the photoswitch performance. Another possible mechanism would be the presence of native GluR hetero-tetramers[36] with subunits displaying different TCP conjugation and photoswitching properties.[12] We cannot rule out the possibility that TCP_{fast} behaves as a positive allosteric modulator or as a partial agonist, allowing only partial receptor activation by partial closure of the ligand binding domain. We argue against this possibility because cis-TCP_{fast} photocurrent in the presence of the orthosteric antagonist DNQX is blocked, and in the presence of glutamate is not reduced, but enhanced, indicating that it is not competing with glutamate.[10,35] In any case, the effect of light in the presence of the endogenous neurotransmitter glutamate can also be envisaged as a way of potentiating physiological rather than generating totally exogenous signals, which is often preferable.

Considering the unique properties of TCP_{fast} to modulate native GluR activity, TCP_{fast} was tested in vivo at the synapse between IHC and SGNs of the cochlea, where excitatory responses are mainly mediated by AMPA receptors.[37,38] TCP_{fast}-mediated control of the SGNs was obtained in minutes by diffusing (and washing out) the compound into the cochlea. Interestingly, neural responses were observed in response to light pulses with energies between 0.5 and 1 μJ, which is the lower range of the optogenetic approaches applied to the adult gerbil cochlea (CatCh: 1−2 μJ,;[39] f-Chrimson: ∼5 μJ).[40] Additionally, maximal oCAP responses were obtained in response to light pulse as short as 80 μs, which is substantially shorter than reported for optogenetic tools in the cochlea.[27,39,41,42] Finally, TCP_{fast} enabled neural responses up to a stimulation rate of 1.5 kHz. Although this observation should be confirmed by single SGN recording, it is interesting to note that this performance is similar to what was reported using an optically evoked auditory brainstem response, for SGNs expressing the fastest opsins to date (Chronos:;[27] vf-Chrimson:[42]), while presenting a lower activation threshold (TCP_{fast} ∼ 1 μJ, Chronos-ES/TS and vf-Chrimson-ES/TS ∼ 6 μJ).

TCP_{fast} provides similar or better performance than current optogenetic approaches in terms of speed and light requirements, while avoiding the gene therapy required to optogenetically modify SGNs. Yet, long-term availability, efficacy, and safety of TCP_{fast} or more advanced photoswitches will need to be established. Moreover, neural degeneration often starts with the loss of postsynaptic structures,[43,44] which may limit the usefulness of TCP_{fast} photopharmacology for optical CIs. Future studies should focus on designing safe compound-targeting channels expressed at the surface of the surviving SGN somas, while showing similar target specificity, fast kinetics, and longer wavelength. This way, photopharmacology might establish a toolkit for photosensitization tailored to the specific neural status of the cochlea or other structures. In addition, a drug-based approach would appeal to patients and the pharmaceutical industry and facilitate regulatory processes. Photopharmacology has previously demonstrated its potential to photosensitize other sensory systems such as the retina.[13,45−47] To the best of our knowledge, this is the first proof-of-concept photopharmacology study in the auditory system and opens up an avenue for auditory research and clinical applications such as in optical CIs designed to fundamentally improve hearing restoration.

EXPERIMENTAL SECTION

Click Reaction. To a 1.5 mL glass vial containing azide **1** ("head", 1.00 mg, 1 equiv) and copper(I) oxide (0.82 mg, 3 equiv) in tetrahydrofuran (47 μL) and equipped with a magnetic stir bar was added a solution of ascorbic acid (1.34 mg, 4 equiv) in water (94 μL) and the resulting mixture was vortexed for 1 min. Then, a solution of alkyne **2** ("tail", 0.47 mg, 1.1 equiv) in tetrahydrofuran (47 μL) was added and the resulting mixture was stirred at room temperature for 45 min. The so obtained final mixture was taken up in dimethylsulfoxide (193 μL), vortexed, centrifuged for 1 min to separate the insoluble copper(I) oxide particles, and finally divided into aliquots of the final compound stock solution (Figure 1B,C and Scheme S2).

https://doi.org/10.1021/jacs.1c12314
J. Am. Chem. Soc. 2022, 144, 9229−9239

Alternatively, the click reaction can be performed in an Eppendorf tube and stirred with a suitable mixer.

We observed that the catalytic performance of the copper(I) oxide may vary significantly from batch to batch, therefore the actual reaction time should be adjusted to obtain at least a 95% conversion of the starting material and a (TCP_{fast}):(hydrolyzed TCP_{fast}) ratio greater than 3 (Figure S12). In vitro and in vivo biological characterizations were done using the same batch and results were reproducible across experiments.

Rat Hippocampal Neural Primary Culture. All experiments were done in compliance with the national animal care guidelines and were approved by the board for animal welfare of the University Medical Center Goettingen and the animal welfare office of the state of Lower Saxony.

Primary hippocampal cultures were prepared from newborn P0−P3 pups Wistar rats. Brains were collected in a 10 cm Petri dish containing ice-cold dissection media (HBSS (Gibco) + 10 mM Hepes (Gibco)). Hippocampi were separated from the brain, and meninges were removed. Hippocampi were digested with 2 mL prewarmed 37 °C 0.1% trypsin−EDTA (Gibco, Germany) for 20 min at 37 °C. Trypsin was removed, and the tissue was washed three times with dissection medium. Dissection medium was replaced with 1 mL prewarmed complete DMEM (DMEM with 1× Glutamax, 10% FCS/FBS and 1% penicillin (100 U/mL)/streptomycin (100 μg/mL); all from Gibco). Tissue was triturated by gentle pipetting. The tissue suspension was filtered through a 100 μm cell strainer (BD Biosciences).

Cells were counted using the trypan blue exclusion method and cultured on 12 mm glass coverslips (Thermo Scientific) coated with poly-D-lysine (Sigma). Neurons were plated in 24-well plates at a density of 50,000 hippocampal neurons per coverslip in 500 μL of NB + medium (Neurobasal with 2% B-27 supplement, 1% Glutamax and 1% penicillin (100 U/mL)/streptomycin (100 μg/mL); all from Gibco) at 37 °C and 5% CO_2. Half of the medium in each well was changed every 3−4 days.

Electrophysiology Recording Conditions for Rat Hippocampal Neurons. Before starting the recording, neurons between 10 and 18 days in vitro (div) were incubated with TCP_{fast} at concentrations: 25−50−75−100 μM (≤2% DMSO) for 2 min, in the absence of light and in pH 9 bath solution composed of (in mM): 100 NaCl, 1 $MgCl_2$, 2.5 KCl, 2.5 $CaCl_2$, 10 glucose, and 50 sodiumcarbonate/sodiumbicarbonate, 310 mOsm/kg, pH 9 adjusted with NaOH.

Voltage and current-clamp recordings under whole-cell configuration were done using an Axopatch 200B amplifier, filtered at 5 kHz, and digitized with an Axon DigiData 1440A interface (Axon Instruments). Acquisition software used was Clampex 10.5.2.6 (Axon Instruments).

Light stimulation was performed at saturating radiant flux (5−14 mW) using diode-pumped solid-state lasers (λ = 473 nm) focused into a 400 μm optic fiber. Light pulses were applied using a fast computer-controlled shutter (Uniblitz LS6ZM2, Vincent Associates, Rochester, USA). Radiant flux was adjusted by placement of density filters between the laser output and the optic fiber.

During recordings, neurons were maintained at room temperature (r.t., 25−27 °C) in a continuous perfusion of bath solution and clamped at −70 mV. Bath solution was composed of (in mM): 140 NaCl, 1 $MgCl_2$, 2.5 KCl, 10 HEPES, 2.5 $CaCl_2$, and 10−20 mM glucose to fix osmolarity to 310 mOsm/kg, pH 7.42 adjusted with NaOH. Borosilicate glass pipettes were pulled with a typical resistance of 3−8 MΩ for neurons. Pipette solution contained (in mM): 129 potassium gluconate, 10 HEPES, 10 KCl, 4 MgATP, and 0.3 Na_3GTP. Osmolarity is adjusted at 289 mOsm/kg, and pH is adjusted to 7.2 with KOH.

Drug Preparation for In Vivo Cochlea Infusion. Artificial perilymph solution consisted of the following (in mM): 137 NaCl; 5 KCl; 2 $CaCl_2$; 1 $MgCl_2$; 1 $NaHCO_3$; and 11 glucose, pH 7.4 adjusted with NaOH and osmolarity: 304 ± 4.3 mOsm/kg. Before each experiment, TCP_{fast} was diluted in artificial perilymph to a final concentration ranging from 2.5 to 12.5 μM.

Animal Preparation for Cochlear Potential Recordings and Cochlear Pharmacology. All experiments were done in compliance with the German national animal care guidelines and were approved by the board for animal welfare of the University Medical Center Göttingen and the animal welfare office of the state of Lower Saxony (agreement 2014/1726 and 2019/3188). Experiments were performed on adult (>8 weeks old) Mongolian gerbils (*Meriones unguicalatus*) of both sexes.

Gerbils were anesthetized by isoflurane (5% for anesthesia induction, 1−3% for maintenance, and frequent testing for the absence of hind-limb withdrawal reflex), and analgesia was obtained by subdermal injection of buprenorphine (0.1 mg/kg body weight) and carprofen (5 mg/kg body weight). Body temperature was maintained at 37 °C using a custom-designed heat plate. The cochlea was exposed following a retroauricular approach and a bullostomy. The recording electrode was placed against the bony edge next to the RW leaving enough space to access the RW for pharmacological manipulation and optical stimulation. The pharmacological manipulation was made by filling the RW niche with the solution of interest. The RW membrane was punctured to increase the fluid exchange between the cochlea and RW niche. Between each solution, the RW niche was emptied by capillarity.

Acoustically Evoked Cochlear Potential. Acoustic cochlear potentials were obtained in response to 8 kHz tone burst (pulse duration = 8 ms, rise/fall time = 1 ms, repetition rate = 20 Hz, level: 20 to 80 dB SPL per 10 dB step, and 200 repetitions per level). The mass potentials were amplified using a custom-made physiological amplifier and sampled at a rate of 50 kHz (NI PCI-6229, National Instrument). Stimulus generation and data acquisition were made using custom-written software (MATLAB, MathWorks) employing National Instrument data acquisition cards in association with a custom-built acoustic and laser-controller.

The cochlear microphonic was extracted by averaging the band-pass filtered (cut-off frequencies = 5.6 and 11.1 kHz) mass potential recorded using the RW electrode and its amplitude defined as the RMS value. The CAP and summating potentials were obtained by averaging the low-pass filtered (cut-off frequency = 3.5 kHz) mass-potential. The CAP amplitude was defined as the amplitude between the first negative peak (N_1) and the following positive peak (P_1). The summating potential amplitude was defined as the difference between the plateau response (between 5 and 7 ms) and the baseline prior to the stimulation onset.

Optically Evoked Cochlear Potential. Optical cochlear potentials were obtained in response to blue light pulse delivered by a 200 μm optical fiber coupled to a 473 nm laser (MLL-FN-473-100, 100 mW, diode pumped solid state [DPSS]; Changchun New Industry Optoelectronics). Irradiance was calibrated with a laser power meter (LaserCheck; Coherent Inc). The CAP was obtained by averaging the low-pass filtered (cut-off frequency = 3.5 kHz) mass potential.

IHC Synapse Counting. Cochleae were fixated in 4% formaldehyde for about 15 min and decalcified in 0.12 M EDTA solution for about 12 h (at 4 °C). Organs of Corti were then: (i) isolated in PBS; (ii) incubated for an hour in Goat serum dilution buffer (GSDB, comprised of: 16% normal goat serum, 450 mM NaCl, 0.3% Triton X-100, 20 mM phosphate buffer, pH 7.4); (iii) treated for 2 h with the primary antibodies: mouse anti-CtBP2 (BD Biosciences, 1:200), rabbit anti-myo6 (Proteus Biosciences, 1:200), and chicken anti-Homer1 (SYsY, 1:200) for staining presynapse, IHCs, and postsynapse, respectively. After washing the primary antibodies with PBS for 20 min, the secondary antibodies were incubated: Goat-anti-Chicken 488 (Invitrogen, 1:500), Goat-anti-Rabbit 568 (Thermo Fisher, 1:500), and Goat-anti-Mouse 647 (Invitrogen, 1:500). After another washing step with PBS, samples were mounted on a glass slide in Mowiol (Carl Roth) mounting medium. Confocal images of the organ of Corti were first obtained using a 10× magnification (LSM 510 microscope, Carl Zeiss, Jena) in order to fit a Greenwood function[48,49] to them and localize the tonotopic position of the IHCs. The synapses were visualized at different tonotopic regions (0.5, 1, 2, 4, 8, 16, and 32 kHz) using a 100× magnification (Abberior

https://doi.org/10.1021/jacs.1c12314
J. Am. Chem. Soc. 2022, 144, 9229−9239

Instruments Expert Line STED microscope) and counted using the spot function from Imaris software (version 7.6.5).

Data Analysis and Statistics. Amplitude of photocurrents was analyzed using IgorPro (Wavemetrics). Displayed whole-cell current traces have been filtered using the infinite impulse response digital filter from IgorPro (low-pass filter with a cutoff of 50 Hz). The drift in current was corrected where appropriate with the IgorPro (WaveMetrics) software using a custom-made macro for drift correction. Statistics were done with OriginPro 8.5 (OriginLab) and Matlab (Mathworks). In vivo electrophysiological data were analyzed using custom-made Matlab routines.

■ ASSOCIATED CONTENT

Supporting Information

The Supporting Information is available free of charge at https://pubs.acs.org/doi/10.1021/jacs.1c12314.

General materials and methods; detailed description of the chemical synthesis and physicochemical characterization of TCP_{fast}; biological in vitro measurements; supporting in vivo method description and measurements; and sequence alignment and molecular docking simulations (PDF)

■ AUTHOR INFORMATION

Corresponding Authors

Tobias Moser − *Institute for Auditory Neuroscience and InnerEarLab, University Medical Center Göttingen, 37075 Göttingen, Germany; Auditory Neuroscience and Optogenetics Group, German Primate Center, 37077 Göttingen, Germany; Cluster of Excellence "Multiscale Bioimaging: from Molecular Machines to Networks of Excitable Cells" (MBExC), University of Göttingen, 37075 Göttingen, Germany*; Email: tmoser@gwdg.de

Pau Gorostiza − *Institute for Bioengineering of Catalonia (IBEC), Barcelona Institute for Science and Technology, 08028 Barcelona, Spain; Network Biomedical Research Center in Bioengineering, Biomaterials, and Nanomedicine (CIBER-BBN), 28029 Madrid, Spain; Catalan Institution for Research and Advanced Studies (ICREA), 08010 Barcelona, Spain*; orcid.org/0000-0002-7268-5577; Email: pau@icrea.cat

Authors

Aida Garrido-Charles − *Institute for Bioengineering of Catalonia (IBEC), Barcelona Institute for Science and Technology, 08028 Barcelona, Spain; Network Biomedical Research Center in Bioengineering, Biomaterials, and Nanomedicine (CIBER-BBN), 28029 Madrid, Spain; Institute for Auditory Neuroscience and InnerEarLab, University Medical Center Göttingen, 37075 Göttingen, Germany; Auditory Neuroscience and Optogenetics Group, German Primate Center, 37077 Göttingen, Germany; Cluster of Excellence "Multiscale Bioimaging: from Molecular Machines to Networks of Excitable Cells" (MBExC), University of Göttingen, 37075 Göttingen, Germany*

Antoine Huet − *Institute for Auditory Neuroscience and InnerEarLab and Auditory Circuit Lab, Institute for Auditory Neuroscience and InnerEarLab, University Medical Center Göttingen, 37075 Göttingen, Germany; Auditory Neuroscience and Optogenetics Group, German Primate Center, 37077 Göttingen, Germany; Cluster of Excellence "Multiscale Bioimaging: from Molecular Machines to Networks of Excitable Cells" (MBExC), University of Göttingen, 37075 Göttingen, Germany*

Carlo Matera − *Institute for Bioengineering of Catalonia (IBEC), Barcelona Institute for Science and Technology, 08028 Barcelona, Spain; Network Biomedical Research Center in Bioengineering, Biomaterials, and Nanomedicine (CIBER-BBN), 28029 Madrid, Spain; Department of Pharmaceutical Sciences, University of Milan, 20133 Milan, Italy*; orcid.org/0000-0001-6939-3859

Anupriya Thirumalai − *Institute for Auditory Neuroscience and InnerEarLab and Auditory Circuit Lab, Institute for Auditory Neuroscience and InnerEarLab, University Medical Center Göttingen, 37075 Göttingen, Germany; Auditory Neuroscience and Optogenetics Group, German Primate Center, 37077 Göttingen, Germany*

Jordi Hernando − *Departament de Química, Universitat Autònoma de Barcelona (UAB), Cerdanyola del Vallès 08193, Spain*; orcid.org/0000-0002-1126-4138

Amadeu Llebaria − *Consejo Superior de Investigaciones Científicas (IQAC-CSIC), Institute of Advanced Chemistry of Catalonia, 08034 Barcelona, Spain*

Complete contact information is available at: https://pubs.acs.org/10.1021/jacs.1c12314

Author Contributions

△A.G.-C., A.H., and C.M. contributed equally to this work. T.M. and P.G. contributed equally to this work.

Notes

The authors declare the following competing financial interest(s): Prof. Dr. Tobias Moser is a co-founder and CEO of OptoGenTech company. The other authors declare no conflict of interests.

■ ACKNOWLEDGMENTS

This research received funding from the European Union Research and Innovation Programme Horizon 2020—Human Brain Project SG3 (945539), DEEPER (ICT-36-2020−101016787), Agency for Management of University and Research Grants/Generalitat de Catalunya (CERCA Programme; 2017-SGR-1442 and 2017-SGR-1604 projects), Fonds Européen de Développement Économique et Régional (FEDER) funds, Ministerio de Ciencia e Innovación, Agencia Estatal de Investigación and ERDF-FEDER European Fund (projects CTQ2017-89222-R and PID2020-120499RB-I00), and Fundaluce and "la Caixa" foundations (ID 100010434, agreement LCF/PR/HR19/52160010). The project Clúster Emergent del Cervell Humà (CECH, 001-P-001682) is cofinanced by the European Union Regional Development Fund within the framework of the ERDF Operational Program of Catalonia 2014−2020 with a grant of 50% of total eligible cost. A.G.-C. was supported by the fellowship BES-2014-068169 and Alexander von Humboldt Foundation. J.H. was supported by Agencia Estatal de Investigación (PID2019-106171RB-100/AEI/10.13039/501100011033) and Generalitat de Catalunya (2017 SGR00465). We thank chemical facility PCB staff (Unai Elezcano, Sònia Varon) and IBEC infrastructure staff (Isabel Oliveira, David Izquierdo). We thank Christiane Senger-Freitag, Sandra Gerke, and Sina Langer for technical support, Gerhard Hoch for his expert technical support, and Patricia Räke-Kügler for excellent administrative support. We thank Thomas Mager for providing the patch clamp setup. This work was funded by the European Research Council through the Advanced Grant "OptoHear" to T.M. under the European Union's Horizon 2020 Research and

Innovation program (grant agreement no. 670759), the Fraunhofer and Max-Planck Cooperation Program (NeurOpto grant) to T.M., was further supported by the German Research Foundation through the Priority Program 1926 "Next generation optogenetics" to A.H. and T.M., and the Leibniz Program (to T.M.) and the Deutsche Forschungsgemeinschaft (DFG, German Research Foundation) under Germany's Excellence Strategy—EXC 2067/1-390729940 to A.H. and T.M. In addition, this research was supported by the Fakultätinternes Forschungförderungsprogramm from the Universitätsmedizin Göttingen, Georg-August-Universität Göttingen to A.H., and Fondation Pour l'Audition (FPA RD-2020-10) to T.M. Molecular graphics and analyses were performed with UCSF Chimera, developed by the Resource for Biocomputing, Visualization, and Informatics at the University of California, San Francisco, with support from NIH P41-GM103311. We thank Dr. Vladimir Belov, Jurgen Bienert, and Jan Seikowski for HPLC and LC−MS measurements of final TCP_{fast} products.

REFERENCES

(1) Kaczmarek, L. K.; Zhang, Y. Kv3 Channels: Enablers of Rapid Firing, Neurotransmitter Release, and Neuronal Endurance. *Physiol. Rev.* **2017**, *97*, 1431−1468.
(2) Grothe, B.; Pecka, M.; McAlpine, D. Mechanisms of Sound Localization in Mammals. *Physiol. Rev.* **2010**, *90*, 983−1012.
(3) Hu, H.; Gan, J.; Jonas, P. Fast-spiking, parvalbumin + GABAergic interneurons: From cellular design to microcircuit function. *Science* **2014**, *345*, 1255263.
(4) Huet, A.; Batrel, C.; Tang, Y.; Desmadryl, G.; Wang, J.; Puel, J.-L.; Bourien, J. Sound Coding in the Auditory Nerve of Gerbils. *Hear. Res.* **2016**, *338*, 32−39.
(5) Moser, T.; Grabner, C. P.; Schmitz, F. Sensory Processing at Ribbon Synapses in the Retina and the Cochlea. *Physiol. Rev.* **2020**, *100*, 103−144.
(6) Kleinlogel, S.; Vogl, C.; Jeschke, M.; Neef, J.; Moser, T. Emerging Approaches for Restoration of Hearing and Vision. *Physiol. Rev.* **2020**, *100*, 1467−1525.
(7) Zeng, F.-G. Challenges in Improving Cochlear Implant Performance and Accessibility. *IEEE Trans. Biomed. Eng.* **2017**, *64*, 1662−1664.
(8) Lenarz, T. Cochlear Implant − State of the Art. *Laryngol., Rhinol., Otol.* **2017**, *96*, S123−S151.
(9) Ankenbruck, N.; Courtney, T.; Naro, Y.; Deiters, A. Optochemical Control of Biological Processes in Cells and Animals. *Angew. Chem., Int. Ed.* **2018**, *57*, 2768−2798.
(10) Gorostiza, P.; Volgraf, M.; Numano, R.; Szobota, S.; Trauner, D.; Isacoff, E. Y. Mechanisms of Photoswitch Conjugation and Light Activation of an Ionotropic Glutamate Receptor. *Proc. Natl. Acad. Sci. U.S.A.* **2007**, *104*, 10865−10870.
(11) Hüll, K.; Morstein, J.; Trauner, D. In Vivo Photopharmacology. *Chem. Rev.* **2018**, *118*, 10710−10747.
(12) Reiner, A.; Isacoff, E. Y. Tethered Ligands Reveal Glutamate Receptor Desensitization Depends on Subunit Occupancy. *Nat. Chem. Biol.* **2014**, *10*, 273.
(13) Izquierdo-Serra, M.; Bautista-Barrufet, A.; Trapero, A.; Garrido-Charles, A.; Díaz-Tahoces, A.; Camarero, N.; Pittolo, S.; Valbuena, S.; Pérez-Jiménez, A.; Gay, M.; García-Moll, A.; Rodríguez-Escrich, C.; Lerma, J.; de la Villa, P.; Fernández, E.; Pericàs, M. À.; Llebaria, A.; Gorostiza, P. Optical Control of Endogenous Receptors and Cellular Excitability Using Targeted Covalent Photoswitches. *Nat. Commun.* **2016**, *7*, 12221.
(14) Harvey, J. H.; Trauner, D. Regulating Enzymatic Activity with a Photoswitchable Affinity Label. *Chembiochem* **2008**, *9*, 191−193.
(15) Volgraf, M.; Gorostiza, P.; Numano, R.; Kramer, R. H.; Isacoff, E. Y.; Trauner, D. Allosteric Control of an Ionotropic Glutamate Receptor with an Optical Switch. *Nat. Chem. Biol.* **2006**, *2*, 47−52.
(16) Gorostiza, P.; Isacoff, E. Optical Switches and Triggers for the Manipulation of Ion Channels and Pores. *Mol. BioSyst.* **2007**, *3*, 686−704.
(17) Gorostiza, P.; Isacoff, E. Y. Optical Switches for Remote and Noninvasive Control of Cell Signaling. *Science* **2008**, *322*, 395−399.
(18) Berlin, S.; Szobota, S.; Reiner, A.; Carroll, E. C.; Kienzler, M. A.; Guyon, A.; Xiao, T.; Trauner, D.; Isacoff, E. Y. A Family of Photoswitchable NMDA Receptors. *eLife* **2016**, *5*, No. e12040.
(19) Kienzler, M. A.; Isacoff, E. Y. Precise Modulation of Neuronal Activity with Synthetic Photoswitchable Ligands. *Curr. Opin. Neurobiol.* **2017**, *45*, 202−209.
(20) Chi, L.; Sadovski, O.; Woolley, G. A. A Blue-Green Absorbing Cross-Linker for Rapid Photoswitching of Peptide Helix Content. *Bioconjugate Chem.* **2006**, *17*, 670−676.
(21) Bandara, H. M. D.; Burdette, S. C. Photoisomerization in Different Classes of Azobenzene. *Chem. Soc. Rev.* **2012**, *41*, 1809−1825.
(22) Kienzler, M. A.; Reiner, A.; Trautman, E.; Yoo, S.; Trauner, D.; Isacoff, E. Y. A Red-Shifted, Fast-Relaxing Azobenzene Photoswitch for Visible Light Control of an Ionotropic Glutamate Receptor. *J. Am. Chem. Soc.* **2013**, *135*, 17683−17686.
(23) Shao, C.; Wang, X.; Xu, J.; Zhao, J.; Zhang, Q.; Hu, Y. Carboxylic Acid-Promoted Copper(I)-Catalyzed Azide-Alkyne Cycloaddition. *J. Org. Chem.* **2010**, *75*, 7002−7005.
(24) Shao, C.; Zhu, R.; Luo, S.; Zhang, Q.; Wang, X.; Hu, Y. Copper(I) Oxide and Benzoic Acid "on Water": A Highly Practical and Efficient Catalytic System for Copper(I)-Catalyzed Azide-Alkyne Cycloaddition. *Tetrahedron Lett.* **2011**, *52*, 3782−3785.
(25) Janssens, N.; Lesage, A. S. J. Glutamate Receptor Subunit Expression in Primary Neuronal and Secondary Glial Cultures. *J. Neurochem.* **2001**, *77*, 1457−1474.
(26) Izquierdo-Serra, M.; Gascón-Moya, M.; Hirtz, J. J.; Pittolo, S.; Poskanzer, K. E.; Ferrer, È.; Alibés, R.; Busqué, F.; Yuste, R.; Hernando, J.; Gorostiza, P. Two-Photon Neuronal and Astrocytic Stimulation with Azobenzene-Based Photoswitches. *J. Am. Chem. Soc.* **2014**, *136*, 8693−8701.
(27) Keppeler, D.; Merino, R. M.; Lopez de la Morena, D.; Bali, B.; Huet, A. T.; Gehrt, A.; Wrobel, C.; Subramanian, S.; Dombrowski, T.; Wolf, F.; Rankovic, V.; Neef, A.; Moser, T. Ultrafast Optogenetic Stimulation of the Auditory Pathway by Targeting-optimized Chronos. *EMBO J.* **2018**, *37*, No. e99649.
(28) Dieter, A.; Keppeler, D.; Moser, T. Towards the Optical Cochlear Implant: Optogenetic Approaches for Hearing Restoration. *EMBO Mol. Med.* **2020**, *12*, No. e11618.
(29) Numano, R.; Szobota, S.; Lau, A. Y.; Gorostiza, P.; Volgraf, M.; Roux, B.; Trauner, D.; Isacoff, E. Y. Nanosculpting Reversed Wavelength Sensitivity into a Photoswitchable IGluR. *Proc. Natl. Acad. Sci. U.S.A.* **2009**, *106*, 6814−6819.
(30) Camarero, N.; Trapero, A.; Pérez-Jiménez, A.; Macia, E.; Gomila-Juaneda, A.; Martín-Quirós, A.; Nevola, L.; Llobet, A.; Llebaria, A.; Hernando, J.; Giralt, E.; Gorostiza, P. Photoswitchable Dynasore Analogs to Control Endocytosis with Light. *Chem. Sci.* **2020**, *11*, 8981−8988.
(31) Garcia-Amorós, J.; Díaz-Lobo, M.; Nonell, S.; Velasco, D. Fastest Thermal Isomerization of an Azobenzene for Nanosecond Photoswitching Applications under Physiological Conditions. *Angew. Chem.* **2012**, *124*, 12992−12995.
(32) Čechová, L.; Filo, J.; Dračínský, M.; Slavov, C.; Sun, D.; Janeba, Z.; Slanina, T.; Wachtveitl, J.; Procházková, E.; Cigáň, M. Polysubstituted 5-Phenylazopyrimidines: Extremely Fast Non-ionic Photochromic Oscillators. *Angew. Chem., Int. Ed.* **2020**, *59*, 15590−15594.
(33) Rullo, A.; Reiner, A.; Reiter, A.; Trauner, D.; Isacoff, E. Y.; Woolley, G. a. Long Wavelength Optical Control of Glutamate Receptor Ion Channels Using a Tetra-Ortho-Substituted Azobenzene Derivative. *Chem. Commun.* **2014**, *50*, 14613−14615.
(34) Prieto, M. L.; Wollmuth, L. P. Gating Modes in AMPA Receptors. *J. Neurosci.* **2010**, *30*, 4449−4459.

https://doi.org/10.1021/jacs.1c12314
J. Am. Chem. Soc. 2022, 144, 9229−9239

(35) Jin, R.; Banke, T. G.; Mayer, M. L.; Traynelis, S. F.; Gouaux, E. Structural Basis for Partial Agonist Action at Ionotropic Glutamate Receptors. *Nat. Neurosci.* **2003**, *6*, 803−810.
(36) Greger, I. H.; Watson, J. F.; Cull-Candy, S. G. Structural and Functional Architecture of AMPA-Type Glutamate Receptors and Their Auxiliary Proteins. *Neuron* **2017**, *94*, 713−730.
(37) Glowatzki, E.; Fuchs, P. A. Transmitter Release at the Hair Cell Ribbon Synapse. *Nat. Neurosci.* **2002**, *5*, 147−154.
(38) Petitpré, C.; Wu, H.; Sharma, A.; Tokarska, A.; Fontanet, P.; Wang, Y.; Helmbacher, F.; Yackle, K.; Silberberg, G.; Hadjab, S.; Lallemend, F. Neuronal Heterogeneity and Stereotyped Connectivity in the Auditory Afferent System. *Nat. Commun.* **2018**, *9*, 3691.
(39) Wrobel, C.; Dieter, A.; Huet, A.; Keppeler, D.; Duque-Afonso, C. J.; Vogl, C.; Hoch, G.; Jeschke, M.; Moser, T. Optogenetic Stimulation of Cochlear Neurons Activates the Auditory Pathway and Restores Auditory-Driven Behavior in Deaf Adult Gerbils. *Sci. Transl. Med.* **2018**, *10*, No. eaao0540.
(40) Huet, A. T.; Dombrowski, T.; Rankovic, V.; Thirumalai, A.; Moser, T. Developing Fast, Red-Light Optogenetic Stimulation of Spiral Ganglion Neurons for Future Optical Cochlear Implants. *Front. Mol. Neurosci.* **2021**, *14*, 635897.
(41) Mager, T.; Lopez de la Morena, D.; Senn, V.; Schlotte, J.; DErrico, A.; Feldbauer, K.; Wrobel, C.; Jung, S.; Bodensiek, K.; Rankovic, V.; Browne, L.; Huet, A.; Jüttner, J.; Wood, P. G.; Letzkus, J. J.; Moser, T.; Bamberg, E. High Frequency Neural Spiking and Auditory Signaling by Ultrafast Red-Shifted Optogenetics. *Nat. Commun.* **2018**, *9*, 1750.
(42) Bali, B.; Lopez de la Morena, D.; Mittring, A.; Mager, T.; Rankovic, V.; Huet, A. T.; Moser, T. Utility of Red-Light Ultrafast Optogenetic Stimulation of the Auditory Pathway. *EMBO Mol. Med.* **2021**, *13*, No. e13391.
(43) Kujawa, S. G.; Liberman, M. C. Adding Insult to Injury: Cochlear Nerve Degeneration after "Temporary" Noise-Induced Hearing Loss. *J. Neurosci.* **2009**, *29*, 14077.
(44) Sergeyenko, Y.; Lall, K.; Liberman, M. C.; Kujawa, S. G. Age-Related Cochlear Synaptopathy: An Early-Onset Contributor to Auditory Functional Decline. *J. Neurosci.* **2013**, *33*, 13686−13694.
(45) Marc, R.; Pfeiffer, R.; Jones, B. Retinal Prosthetics, Optogenetics, and Chemical Photoswitches. *ACS Chem. Neurosci.* **2014**, *5*, 895−901.
(46) Yue, L.; Weiland, J. D.; Roska, B.; Humayun, M. S. Retinal Stimulation Strategies to Restore Vision: Fundamentals and Systems. *Prog. Retin. Eye Res.* **2016**, *53*, 21−47.
(47) Tochitsky, I.; Kienzler, M. A.; Isacoff, E.; Kramer, R. H. Restoring Vision to the Blind with Chemical Photoswitches. *Chem. Rev.* **2018**, *118*, 10748−10773.
(48) Greenwood, D. D. Critical Bandwidth and the Frequency Coordinates of the Basilar Membrane. *J. Acoust. Soc. Am.* **1961**, *33*, 1344−1356.
(49) Müller, M. The Cochlear Place-Frequency Map of the Adult and Developing Mongolian Gerbil. *Hear. Res.* **1996**, *94*, 148−156.

https://doi.org/10.1021/jacs.1c12314
J. Am. Chem. Soc. 2022, 144, 9229−9239